Applied Catalysis B: Environmental 152–153 (2014) 383–389

Contents lists available at ScienceDirect

Applied Catalysis B: Environmental

journal homepage: www.elsevier.com/locate/apcatb

# Selective oxidation of benzene to phenol by Fe-CN/TS-1 catalysts under visible light irradiation

Xiangju Ye, Yanjuan Cui, Xiaoqing Qiu, Xinchen Wang*

*State Key Laboratory of Photocatalysis on Energy and Environment, College of Chemistry and Chemical Engineering, Fuzhou University, Fuzhou 350002, P. R. China*

ARTICLE INFO

*Article history:*
Received 21 November 2013
Received in revised form 18 January 2014
Accepted 26 January 2014
Available online 2 February 2014

*Keywords:*
Carbon nitride
Titanium silicate zeolite
Oxidation of benzene
Photosynthesis
Phenol

ABSTRACT

Fe-g-$C_3N_4$ (denoted as Fe-CN) and titanium silicate zeolite (TS-1) hybrid materials were fabricated by a facial thermal polymerization approach using dicyandiamide, metal chloride as precursors and TS-1 zeolite as a support. The structure and textural properties of the resulting hybrid materials were thoroughly characterized by X-ray diffraction, UV–Vis spectrophotometry, nitrogen adsorption–desorption isotherm, Fourier transform infrared spectroscopy, scanning transmission electron microscopy, X-ray photoelectron spectroscopy and electrochemical measurement. The as-synthesized Fe-CN/TS-1 composites could be used as heterogeneous catalysts for the photocatalytic selective oxidation of benzene to phenol using $H_2O_2$ as benign oxidant under ambient conditions. It is found that the Fe-CN/TS-1 hybrid materials show superior photocatalytic performance for the phenol production from benzene to sole Fe-CN and TS-1 catalysts. Under the optimal conditions, up to 10.0% phenol yield (based on benzene) is achieved over the hybrid materials, with 18.4% phenol selectivity (based on $H_2O_2$).



## 1. Introduction

Phenol is one of the most important intermediates in the chemical industry, because it can be further used as intermediates to synthesize many important compounds such as bisphenol A, nylon-6, dyes and so on [1]. Generally, the well-known Fenton reagent ($Fe^{2+}$–$H_2O_2$) has been traditionally used to catalyze benzene to phenol conversion. Unfortunately, this homogeneous reaction system causes difficulty in the separation of catalysts from the reaction products [2]. In addition, the dependence on the strong acids during the catalytic process leads to the corrosion of the reaction apparatus [3,4]. To meet the increasing demand of phenol and to satisfy environmental protection requirements, many efforts have been devoted towards phenol production from benzene, including the electrochemical and catalytic oxidation approaches [5–10]. For example, oxidation of benzene to phenol in the gas phase using several clean oxidants, such as $N_2O$ [11,12], $O_2$ [13–17], air/CO [1] and $H_2/O_2$ [18,19] have been reported. Although good phenol yield is achieved in such optimized approach, this process suffers from rapid deactivation of catalysts on account of the coke formation under high-temperature conditions (300–500 °C) [20–22]. Selective oxidation of benzene to phenol under mild conditions remains a big chemical challenge.

Heterogeneous catalysts have recently been employed for the direct hydroxylation of benzene to phenol with $H_2O_2$, including Fe-containing zeolite [23–25], titanium-containing molecular sieves [26,27], and vanadium-containing porous materials [28,29]. Among these, it is reported that the catalytic activity of titanium-containing zeolite comes from the specific features of isolated Ti active sites that activate hydrogen peroxide [30,31]. Unfortunately, the process for transformation of benzene to phenol is usually limited by its poor selectivity, since phenol is thermodynamically easier to be oxidized completely into $CO_2$ and $H_2O$ [32,33]. Photocatalysis on the selective organic transformations based on the utilization of solar energy provides an alternative pathway for green synthesis using abundant solar irradiation [34–37]. $TiO_2$ photocatalyst has been used for the phenol synthesis from benzene [32,33]. However, the reaction system must be performed under UV light irradiation, which accounts for only 3–4% of the incoming sunlight on the Earth. This significantly restricts its photochemical applications. Therefore, the development of visible-light-active photocatalysts for phenol production from benzene is highly desirable.

Most recently, graphitic carbon nitride (g-CN) materials synthesized typically by the thermal-indcued polymerization of dicyandiamide (Scheme 1) have been introduced as stable and sustainable heterogeneous catalysts that have already shown promising applications in several important fields, such as photolysis of water [38–42], organic photosynthesis [43,44], reduction of $CO_2$ [45], photodegradation of organic pollutants [46] and so on. In our previous studies, we found that mesoporous graphitic carbon

* Corresponding author. Tel.: +86 59183920097; fax: +86 591 83738608.
*E-mail address:* xcwang@fzu.edu.cn (X. Wang).

0926-3373/$ – see front matter © 2014 Elsevier B.V. All rights reserved.
http://dx.doi.org/10.1016/j.apcatb.2014.01.050

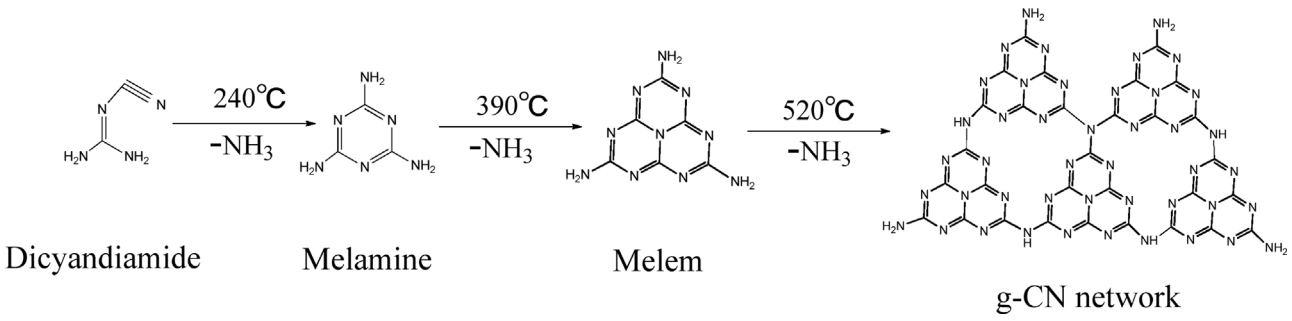


**Scheme 1.** Thermal polymerization of dicyandiamide to g-CN network.

nitride (mpg-CN) could photocatalyze a single-step oxidation of benzene to phenol with $H_2O_2$ under visible light irradiation. After doping with iron ions, the catalytic activity of the resultant Fe-CN was improved significantly. To further improve the catalytic activity, mesoporous silicate zeolite SBA-15 was selected as a support to increase the surface reactive sites [23,47]. TS-1 zeolite is a recommended choice as it has already been found interesting application in the activation of $H_2O_2$ to catalyze the hydroxylation of benzene to phenol [27]. Herein, we investigate the support effect of zeolitic materials on Fe-CN photocatalysis towards the synthesis of phenol from the direct oxidation of benzene using $H_2O_2$ as a clean oxidant.

The Fe-CN/TS-1 hybrid catalysts were synthesized by a facial thermal polymerization approach using dicyandiamide, metal chloride as precursors and TS-1 zeolite as a support. The catalytic activities of the resulting materials were evaluated by the oxidation of benzene to phenol under visible light irradiation in a biphasic water–$H_2O_2$/acetonitrile medium. The results show that these hybrid materials afford a high photocatalytic activity towards the conversion of benzene at mild conditions.

## 2. Experimental

TS-1 zeolite with molar ratio Ti/Si of 0.025–0.033 was purchased from Novel Chemical Technology Co. Ltd. (Shanghai, China). Dicyandiamide was supplied by Sigma Aldrich. Iron(III) chloride, copper chloride, zinc chloride, cobalt chloride, nickel chloride, acetonitrile, benzene, toluene, and hydrogen peroxide (30 wt%) were purchased from Sinopharm Chemical Reagent Co., Ltd. (Shanghai, China). All of the materials were used as received without further purification.

### 2.1. Preparation of Fe-CN

Fe-CN was prepared according to the report [23]. 1 g dicyandiamide mixed with 10 ml deionized water was stirred and heated at 373 K with different amounts of $FeCl_3$ added until the removal of water, forming a reddish solid. The powder was grounded in a mortar, transferred into a crucible and heated under flowing nitrogen atmosphere at 2.3 K/min (4 h) up to 823 K and then held at this temperature for another 4 h, followed by naturally cooling to room temperature.

### 2.2. Preparation of Fe-CN/TS-1

Fe-CN/TS-1 hybrid samples were prepared as follows: different amounts of dicyandiamide were dissolved in 20 ml deionized water mixed with $FeCl_3$ and stirred at 373 K. Then, 1.0 g TS-1 was added into the mixture. After the water was removed, the as-obtained powder was heated at 2.3 K/min (4 h) up to 823 K for 4 h under flowing nitrogen atmosphere, followed by naturally cooling to room temperature. The samples were denoted as Fe-CN/TS-1-*X*, where *X* is an arbitrary number that represents the weight ratio of $FeCl_3$/dicyandiamide or dicyandiamide/TS-1 zeolite. Other compounds with different metals coupled (M-CN/TS-1), including Cu-CN/TS-1, Ni-CN/TS-1, Zn-CN/TS-1 and Co-CN/TS-1 were synthesized similarly.

### 2.3. Sample characterization

X-ray diffraction (XRD) patterns of the samples were collected by using a Bruker D8 Advance X-ray diffractometer (Cu-*K*α1 irradiation, λ = 1.5406 Å). Fourier transformed infrared (FT-IR) spectra were recorded on a Nicolet Magna 670 FTIR spectrometer and the samples were mixed with KBr at a concentration of ca. 1 wt%. A Varian Cary 500 Scan UV–Vis spectrophotometer was used to record the UV–Vis diffuse reflectance spectra of different samples with barium sulfate as the reference sample. $N_2$ adsorption–desorption analyses were carried out at 77 K by a Mocromeritics ASAP 2010 Surface Area and Porosity Analyzer. For obtaining TEM images, the as-obtained samples were examined using a JEOL 2010F scanning transmission electron microscope (STEM) equipped with a field emission gun electron source operated at 200 kV (JEOL, Japan). X-ray photoelectron spectroscopy (XPS) measurements were performed on a Thermo Scientific ESCA Lab 250 spectrometer which consists of a monochromatic Al *K*α as the X-ray source a hemispherical analyzer and sample stage with multi-axial adjustability to obtain the composition on the surface of samples. All the binding energies were calibrated by the C 1s peak of the surface adventitious carbon at 284.7 eV.

Electrochemical measurements were carried out on a BAS Epsilon workstation using a conventional three-electrode, which were immersed in the solution of 0.2 M $Na_2SO_4$ (30 ml, pH = 6.8). The Fe-CN/TS-1 electrodes were employed as the working electrodes, which were prepared on indium-tin oxide (ITO) conductor glasses. The 10 mg sample was dispersed in 400 μl *N*,*N*-dimethylformamide with 1 wt% Nafion solution by sonication to get a slurry mixture. The slurry was spread onto ITO glass whose side part was previously protected by a Scotch tape. The working electrode was dried overnight under ambient conditions. A copper wire was connected to the side part of the working electrode using a conductive tape. Uncoated parts of the electrode were isolated with epoxy resin. Pt and Ag/AgCl electrode were used as a reference and a counter electrode, respectively. A 300 W Xe lamp was applied as the excitation light source with a UV band-pass filter (>420 nm).

The measurements of the amount of $^{\bullet}OH$ were performed for the Fe-CN/TS-1 photocatalytic reaction in the presence of $H_2O_2$ by means of a terephthalic acid-fluorescence (TA-FL) probing method, which emitted fluorescence at around 426 nm on the excitation of its own 312 nm absorption band. An aqueous solution containing 10 mmol NaOH and 5 mmol terephthalic acid (TA) was prepared, and then 40 mg of Fe-CN/TS-1 powder was suspended in 80 ml of

this solution with 0.01 M $H_2O_2$ solution. At several min intervals, 4 ml aliquots were sampled and centrifuged to remove the catalysts. The photoluminescence intensity of 2-Hydroxyl-terephthalic acid (TAOH) was surveyed by an Edinburgh FL/FS 900 spectrophotometer. The fluorescence (PL) was excited with a Xenon lamp with 450 W electric powers in conjunction with a cut-off filter ($\lambda > 420$ nm).

### 2.4. Photocatalytic activity test

To evaluate the catalytic/photocatalytic activities of the Fe-CN/TS-1 samples, the catalytic oxygenation tests of benzene to phenol were carried out via the following method reported in the literature [23]. Fe-CN/TS-1 (50 mg) was suspended in a mixture of acetonitrile (4 ml), benzene (0.8 ml, 9 mmol), water (4 ml) and hydrogen peroxide (30 wt%, 0.51 ml, 5 mmol). The resulting biphasic system was stirred at 333 K for 4 h in the dark. At the end of the reaction, ethanol (5 ml) was poured into the mixture at 277 K for quenching the reaction and to turn the biphasic system to a single-phase system. To carry out the photochemical reactions, a 300 W Xenon lamp together with a 420 nm cut-off filter was used as a visible light source for the irradiation of reaction systems, with otherwise the same experimental conditions as those in the dark. The products of the reactions were analyzed by a high performance liquid chromatography (HPLC 2487, C18, 150 mm × 4.6 mm, id = 5 μm) with toluene as the internal standard. The concentration of $H_2O_2$ was determined by a colorimetric titration method based on the formation of a yellow coloured complex $Ti^{IV}$–$H_2O_2$, using a UV/Vis spectrophotometer at 410 nm.

## 3. Results and discussions

### 3.1. Physicochemical properties of Fe-CN/TS-1

XRD analysis is used to determine the structure of the synthesized composite samples, and the results are shown in Fig. 1a. Consistent with our previous reports that for the Fe-CN sample [48], two typical peaks at 13.0° and 27.4° are observed, which are indexed as (0 0 2) and (1 0 0) diffraction of g-CN structure, respectively. The diffraction peaks of TS-1 belong to orthorhombic symmetry, corresponding to the MFI zeolitic structure [49]. After nanocoating Fe-CN on TS-1 zeolite, it can be obviously found that the intensity of typical diffraction peaks belonging to TS-1 decreases sharply, signifying that the well-defined MFI structure is somewhat destroyed after sintering the hybrid materials. This result suggests that the guest species (Fe-CN) are successfully decorated on the surface of TS-1. Additionally, the interlayer peak of g-CN at 27.4° disappears, possibly because of its low content or a thin-layer of CN formed in the structure of TS-1.

FT-IR spectra of Fe-CN, TS-1 and composite sample are shown in Fig. 1b. For Fe-CN, typical bands of aromatic CN heterocycles at 1200 to 1600 $cm^{-1}$ and the triazine units at 800 $cm^{-1}$ are observed. The broad band at around 3000 $cm^{-1}$, corresponding to secondary and primary amines associated with incomplete graphitic condensation, is also observed in the spectra of the Fe-CN. TS-1 exhibits an absorption band at about 960 $cm^{-1}$, which is related to the stretching vibration of $SiO_4$ units bound to Ti atoms. The vibrational mode at 1633 $cm^{-1}$ is obviously enhanced after Fe-CN decoration, indicating the presence of Fe-CN on the surface of TS-1. The optical properties of a series of Fe-CN/TS-1 catalysts were characterized by UV–Vis spectrometer. As shown in Fig. 2, TS-1 shows its characteristic absorption band around 230 and 290 nm in the UV–Vis spectrum, which demonstrates the existence of distorted tetrahedral and reversible penta-coordinated Ti species in TS-1 [50]. With increasing in the content of Fe-CN, a remarkable redshift of optical

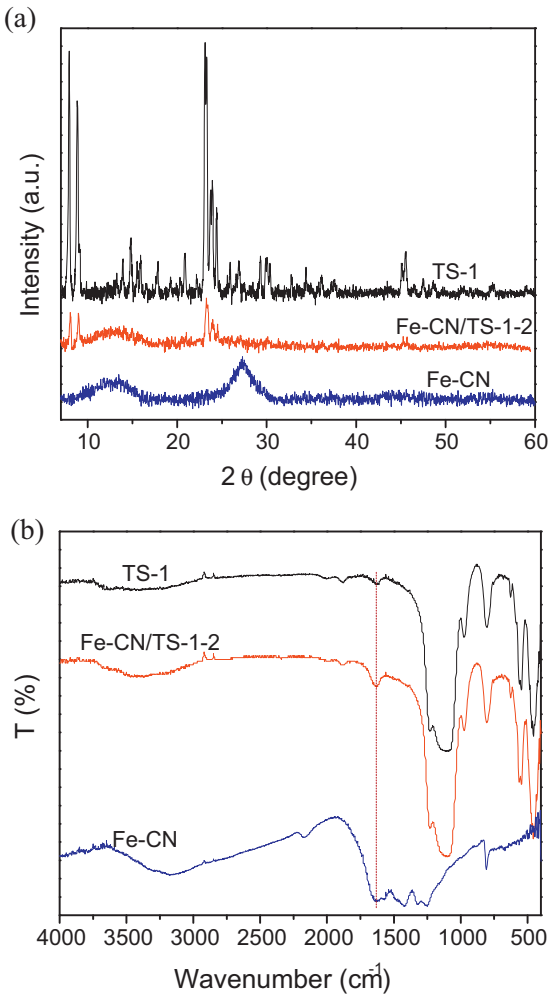


**Fig. 1.** Powder XRD patterns (a) and FT-IR spectra (b) of TS-1, Fe-CN and Fe-CN/TS-1–2 samples.

absorption of the composite samples can be found. Simultaneously, the light absorption intensity not only in visible but UV range is significantly strengthened. This extended absorption wavelength of sunlight is beneficial for enhancing the photocatalytic activity for the conversion of benzene.

The texture and structure of samples were evaluated by nitrogen adsorption–desorption measurements (Fig. 3). The specific surface area of sample Fe-CN/TS-1–2 is 266 $m^2/g$, which is slightly lower

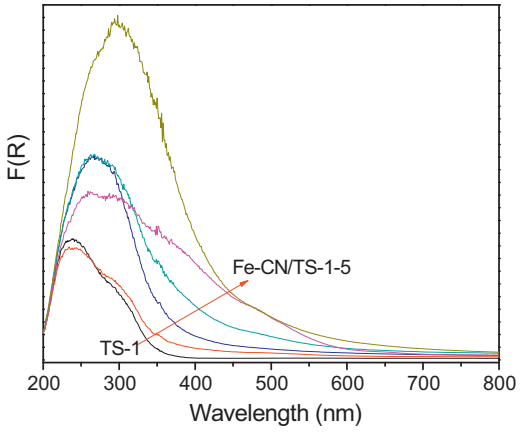


**Fig. 2.** Optical absorption spectra of TS-1 and Fe-CN/TS-1.

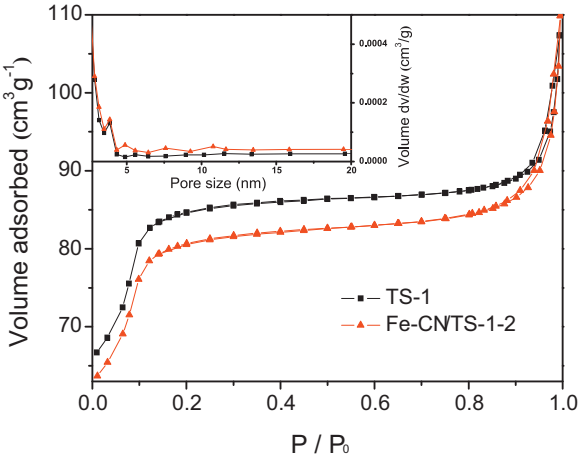


**Fig. 3.** $N_2$ adsorption–desorption isotherms for TS-1 and Fe-CN/TS-1–2. The inset is the corresponding BJH pore-size distribution curves.

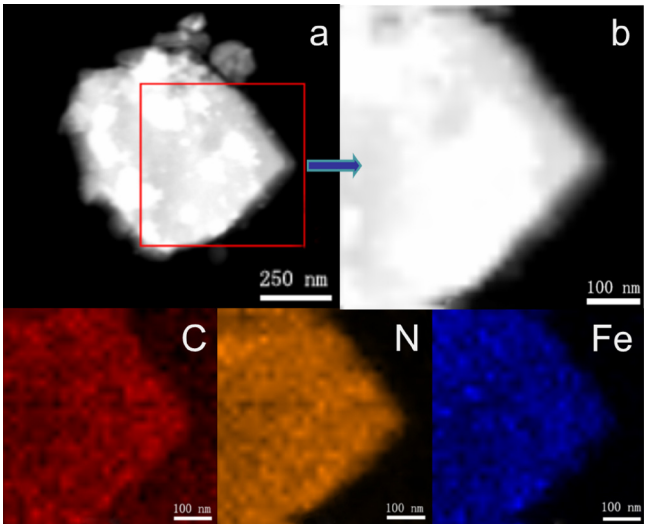


**Fig. 5.** Typical STEM dark field images of Fe-CN/TS-1 (a and b) and the corresponding elemental mapping images of C, N, and Fe.

than that of TS-1 (279 $m^2$/g). This may be attributed to the fact that the deposition of Fe-CN would block the some portion of pores of the TS-1. In addition, the average pore width and pore volume of the composite sample are very close to the initial parameters of TS-1, which indicates the homogeneous dispersion of Fe-CN in the surface and internal pore structure.. The surface chemistry homogeneity of Fe-CN/TS-1 hybrid catalysts was analyzed by elemental mapping technology, which clearly visualized the homogeneous incorporation of Fe-CN onto the microstructure titanium silicate zeolite. The corresponding elemental mapping of C, N and Fe was carried out on a carbon-coated Cu grid, which further verified that the C, N and Fe atoms were uniformly distributed throughout the TS-1 zeolitic frameworks (Fig. 5 ). The elemental state of Fe species on the surface of the Fe-CN/TS-1–2 before and after the catalytic reaction were investigated by XPS. As seen in Fig. 6, the Fe 2p spectra consist of two high-resolution peaks located at 711.3 and 724.6 eV, corresponding to Fe $2p_{3/2}$ and Fe $2p_{1/2}$ of $Fe^{3+}$, respectively, which is in good agreement with the previous literature reports [23,37].

The migration of the photo-generated charge-carriers of material are an important process in photocatalytic reaction, which can be studied by (photo)electrochemical experiments [51,52]. In Fig. 7a, a significant decrease in semicircular Nyquist plots is observed for Fe-CN-decorated samples in dark, clearly demonstrating that the deposition of Fe-CN can evidently improve the electronic conductivity of TS-1 zeolite and promote the charge separation. In addition, periodic on/off photocurrent response was performed under visible light irradiation in a conventional three-electrode electrochemical cell. As shown in Fig. 7b, it is seen that TS-1 shows negligible photocurrent under visible light irradiation due to its insulator nature. In contrast, Fe-CN-modified TS-1 exhibits significantly enhanced photocurrent, as compared with the bared TS-1, which again reflects the coating of Fe-CN on the framework of TS-1.

Based on the above discussions on the physical and (photo)electrochemical properties of TS-1 and Fe-CN/TS-1, we may conclude that homogeneous Fe-CN thin film (at certain loading amount) is successfully introduced into the zeolitic nanoarchitecture of TS-1 without blocking its pore channels. The open microporous structure of TS-1 zeolite is favourable for light harvesting and mass transfer in photocatalysis process.

### 3.2. Photocatalytic oxidation of benzene to phenol by Fe-CN/TS-1 composites

The activity tests of benzene hydroxylation were carried out with a series of Fe-CN/TS-1 catalysts in a biphasic water–$H_2O_2$/acetonitrile medium in a self-pressurized glass reactor using $H_2O_2$ as oxidant under mild conditions (60 °C and

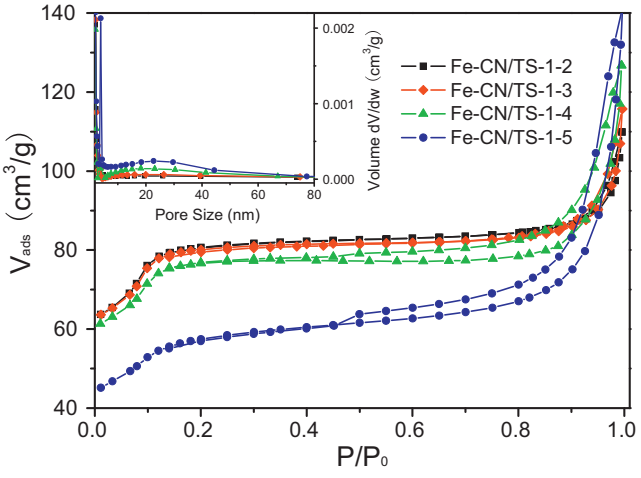


**Fig. 4.** $N_2$ adsorption–desorption isotherms for Fe-CN/TS-1 with different amount of Fe-CN. The insert is the corresponding BJH pore-size distribution curves.

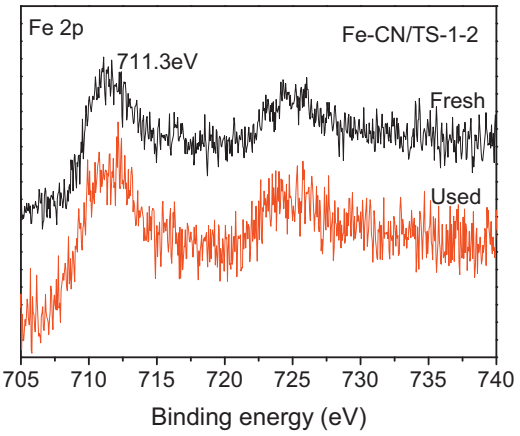


**Fig. 6.** High-resolution Fe 2p XPS spectra of Fe-CN/TS-1–2 before and after the catalytic reaction.

**Table 1**
Catalytic performance of Fe-CN/TS-1 for the direct synthesis of phenol with (+) and without (−) visible light (λ > 420 nm)[a].

| Entry | Catalyst | hυ | Yield[b] (%) | | | PH Sel.[c] (%) | $H_2O_2$ Conv.[d] (%) | |
|---|---|---|---|---|---|---|---|---|
| | | | PH | CA | HQ | BQ | | |
| 1 | Fe-CN | − | 0.4 | t. a.[e] | t. a. | t. a. | 5.0 | 15.2 |
| 2 | | + | 1.1 | t. a. | t. a. | 0.1 | 2.3 | 100 |
| 3 | TS-1 | − | 1.4 | t. a. | t. a. | t. a. | 35.1 | 5.2 |
| 4 | | + | 2.4 | t. a. | t. a. | t. a. | 41.3 | 11.5 |
| 5 | Fe-CN/TS-1–1 | + | 2.8 | t. a. | 0.9 | 2.1 | 5.4 | 98.4 |
| 6 | Fe-CN/TS-1–2 | − | 2.4 | t. a. | t. a. | 0.4 | 13.7 | 32.6 |
| 7 | | + | 10.0 | t. a. | 0.4 | 1.8 | 18.4 | 99.3 |
| 8 | Fe-CN/TS-1–3 | + | 8.8 | t. a. | 1.0 | 1.3 | 16.4 | 100 |
| 9 | Fe-CN/TS-1–4 | + | 1.3 | t. a. | t. a. | t. a. | 2.3 | 100 |
| 10 | Fe-CN/TS-1–5 | + | 0.1 | t. a. | t. a. | t. a. | 0.3 | 100 |
| 11 | Fe-CN/SBA-15–2 | + | 4.7 | t. a. | t. a. | 0.7 | 13.5 | 65.1 |
| 12 | – | + | 0 | 0 | 0 | 0 | 0 | 3.1 |
| 13 | Fe/TS-1 | + | 7.6 | t. a. | 0.9 | 2.1 | 14.6 | 95.6 |

[a] Reaction conditions, see Section 2. Fe-CN/TS-1-*X* (*X* = 1, 2, 3, 4, 5 for 10%, 20%, 50%, 100%, 200% dicyandiamide/TS-1).
[b] Moles of product/moles of initial benzene × 100. PH is the phenol, CA is the catechol, HQ is the hydroquinone, BQ is the benzoquinone.
[c] Moles of produced phenol/moles of reacted $H_2O_2$ × 100.
[d] Moles of reacted $H_2O_2$/moles of initial $H_2O_2$ × 100.
[e] Trace amount.

pH = 7), in which the synthetic phenol was extracted from water into organic phase in order to minimize per-oxidation [3]. For full understanding, the effect of various conditions including different amounts of Fe-CN, iron element and different metal precursors on the direct oxidation of benzene to phenol was investigated.

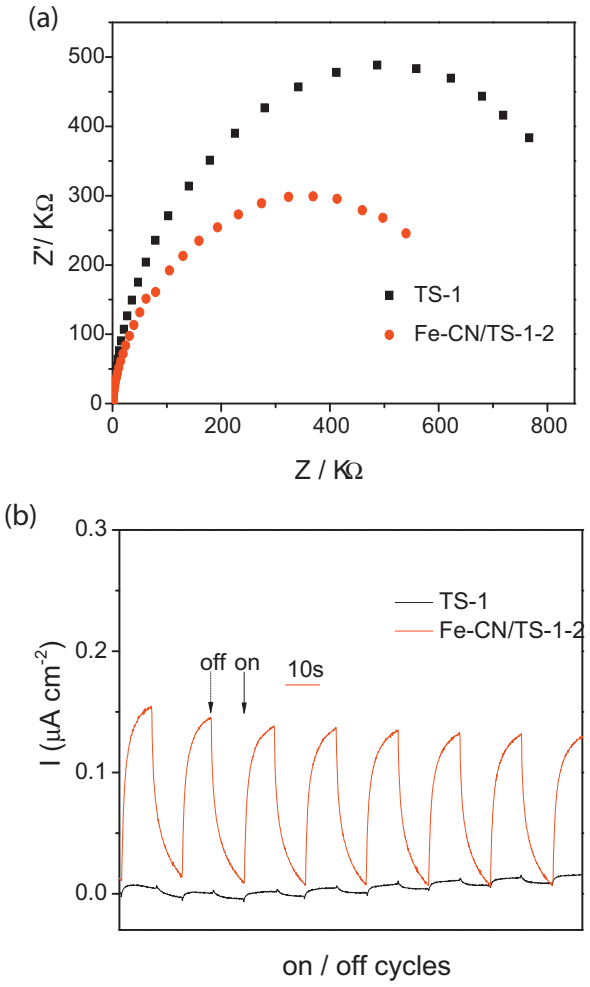


**Fig. 7.** Photoelectrochemical properties of TS-1 and Fe-CN/TS-1–2 samples in a 0.2 M $Na_2SO_4$ aqueous solution (PH = 6.8). Electrochemical impedance spectroscopy plots in the dark (a) and the periodic on/off photocurrent response under visible light irradiation (b).

As listed in Table 1, no detectable activity in the absence of catalyst and low activity in the dark well confirms that it indeed goes through photocatalytic hydroxylation of benzene to phenol with Fe-CN/TS-1 composites (entries 12, 6 of Table 1). In the case of sole Fe-CN and TS-1 catalyst under visible light irradiation (entries 2 and 4 of Table 1), the yields of phenol based on benzene are only 1.1% and 2.4%, respectively. For the Fe-CN/TS-1 composite catalysts, with the increase of Fe-CN content, the production of phenol increases and then drastically decreases. The best catalytic activity of 10.0% phenol yield and good selectivity (18.4% based on $H_2O_2$) is obtained on Fe-CN/TS-1–2. It is much higher than the simple sum of the phenol yield on sole Fe-CN and TS-1 catalyst and about 9 and 4 times higher than that of them, respectively. Furthermore, from the texture parameter of the as-synthesized samples and their activities (Fig. 4 and Table 2), we can find that the micro pore volume and surface area gradually decrease with the increase in the loading amount of Fe-CN on the TS-1 support, which leads to the decrease of catalytic activity. Meanwhile, the content of iron also affect their catalytic activity. When the content of iron is too high, the self-decomposition of hydrogen peroxide induced by the iron catalyst would reduce phenol yield. Contrast to the catalyst support with the same composite but SBA-15 no TS-1, only 4.7% phenol yield based on benzene is gained (entry 11 of Table 1). This may be attributed to the fact that TS-1 not only offers a support to improve the exposure of catalytic sites, but also acts as a catalyst for benzene conversion, which leads to the synergistic effect between Fe-CN and TS-1zeolite. A reference experiment was performed by Fe/TS-1 mixture (entry 13 of Table 1), a moderate phenol yield (7.6%) was obtained. However, it is still lower than the as-obtained composites (Fe-CN/TS-1–2) under the same reaction conditions. This is due to the fact that carbon nitride acts as a visible light transducer to generate energized electron-hole pairs for visible light photoredox catalysis. Some minor by-products (such as catechol,

**Table 2**
The relationship between the textural parameters and the photocatalytic activity of the samples.

| Sample | Surface area ($cm^2/g$) | Micro pore volume ($cm^3/g$) | Phenol yield (%) |
|---|---|---|---|
| Fe-CN/TS-1–2 | 266 | 0.076 | 10.0 |
| Fe-CN/TS-1–3 | 264 | 0.075 | 8.8 |
| Fe-CN/TS-1–4 | 253 | 0.069 | 1.3 |
| Fe-CN/TS-1–5 | 191 | 0.045 | 0.1 |

**Table 3**
Catalytic performance of Fe-CN/TS-1 with different iron content for the direct synthesis of phenol with visible light ($\lambda > 420$ nm)[a].

| Entry | Catalyst | $t$ (h) | Yield (%) | | | PH Sel. (%) | $H_2O_2$ Conv. (%) | |
|---|---|---|---|---|---|---|---|---|
| | | | PH | CA | HQ | BQ | | |
| 1 | Fe-CN/TS-1–6 | 4 | 1.4 | t. a. | t. a. | t. a. | 23.2 | 10.3 |
| 2 | Fe-CN/TS-1–2 | 4 | 10.0 | t. a. | 0.4 | 1.8 | 18.4 | 99.3 |
| 3 | Fe-CN/TS-1–7 | 4 | 5.0 | t. a. | t. a. | 0.3 | 9.6 | 100 |
| 4 | Fe-CN/TS-1–8 | 4 | 1.6 | t. a. | t. a. | t. a. | 3.0 | 100 |

[a] Reaction conditions, see Section 2. Fe-CN/TS-1-$X$ ($X$ = 6, 2, 7, 8 for 5%, 10%, 20%, 50% $FeCl_3$/dicyandiamide).

hydroquinone and benzoquinone) were also detected in the reaction products since the imbalance between the decomposition rate of $H_2O_2$ and the oxidation rate of benzene during the liquid phase benzene oxidation process.

Iron as an ideal catalytic element plays an important catalytic role in the phenol production from benzene with $H_2O_2$. To evaluate the effect of iron content in our synthesized catalysts for the transformation of benzene to phenol, Fe-CN/TS-1 samples with different iron contents were prepared and the results of the catalytic activities were summarized in Table 3. With the increase of iron content, benzene conversion enhances and subsequently decreases. The maximal phenol yield (10.0%) is obtained on the catalyst with 10 wt% iron deposition. This observation can be interpreted as follows. The presence of more active iron species in the reaction system causes more production of necessary hydroxyl radicals, and then more phenol is synthesized from benzene in the presence of $H_2O_2$. However, when excess amount of iron species is decorated on carbon nitride, the self-decomposition of hydrogen peroxide induced by the presence of more iron catalyst would cause the decreased yield of phenol. Meanwhile, the selectivity of the phenol slightly decreases. It is attributed to more by-products (such as catechol, hydroquinone, benzoquinone), which is formed during the photocatalytic reaction.

After the reaction, the Fe-CN/TS-1–2 catalyst was recovered, washed, and then respersed in a new reaction mixture for a second operation of the reaction. It was found that the phenol yield decreased from 10.0% to 6.0%. An improvement in the interaction of the Fe-CN catalytic active phase with the TS-1 host is needed in our future work.

It should be noted that other transition metal besides Fe are also active towards benzene hydroxylation. To our knowledge, the transition metal element could always not be ignored in catalytic chemistry. In order to investigate the effect of other metal elements coupled in our composite catalysts (M-CN/TS-1) for phenol production, we prepared a series of catalysts through the same method but with different transition metal elements. The results of the catalytic activities are listed in Table 4. From the table, we can see that in contrast to Fe-CN/TS-1 composite catalysts, no improvements of the activities are observed in these samples. A lower phenol yield is obtained by composite catalysts modified with other transition metal elements (e.g. Cu, Zn, Co, Ni). The activity sequences of the different metal deposited catalysts follow the orders: Fe > Cu > Ni > Zn > Co. Furthermore, the order of the $H_2O_2$ conversion rate is consistent with that of phenol yield. These results reveal that iron ions are the most active species for the selective oxidation of benzene to phenol under ambient conditions.

Since •OH species are playing important role in the photocatalytic benzene oxidation process, TA-PL probing technique is utilized to investigate the •OH radical generation in the presence of the hydrogen peroxide under visible light irradiation. It is known that •OH reacts with TA to generate TAOH, which emits an unique fluorescence signal with a peak at 426 nm [53,54]. The •OH-trapping PL spectra of suspensions containing TS-1 and TA, Fe-CN/TS-1–2 and TA in the presence of $H_2O_2$ are shown in Fig. 8. A steady improvement of the photoluminescence intensity are obtained by TS-1 and Fe-CN/TS-1–2 under visible light irradiation, respectively. More importantly, the intensities at 426 nm of Fe-CN/TS-1–2 are much higher than those of TS-1 against the irradiation time. These results strongly suggest that the hydroxyl radicals are indeed generated in TS-1 and Fe-CN/TS-1–2 catalytic systems

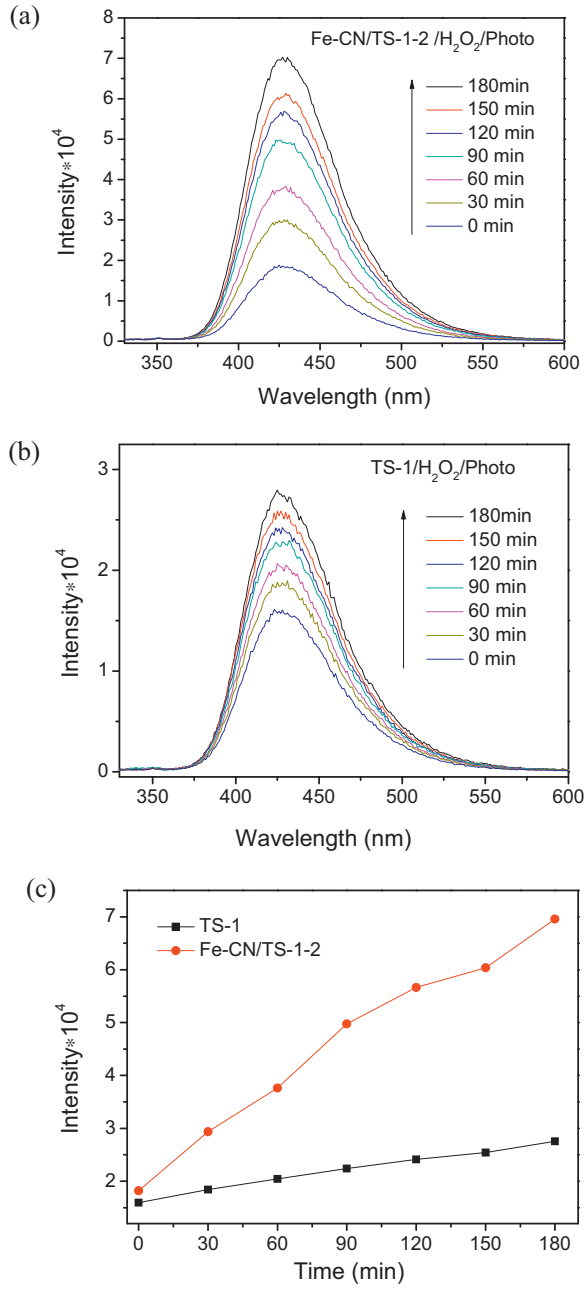


**Fig. 8.** The OH-trapping PL spectra of suspensions containing Fe-CN/TS-1–2/$H_2O_2$, TA (a) and TS-1/$H_2O_2$, TA (b). Plot of the induced PL intensity (at 426 nm) against reaction time with TS-1 and Fe-CN/TS-1–2 under visible light irradiation (c).

**Table 4**
Catalytic performance of M-CN/TS-1–2 deposited with different transition metals for the direct synthesis of phenol with visible light (λ > 420 nm)[a].

| Entry | Catalyst | t (h) | Yield (%) | | | | PH Sel. (%) | $H_2O_2$ Conv. (%) |
|---|---|---|---|---|---|---|---|---|
| | | | PH | CA | HQ | BQ | | |
| 1 | Fe-CN/TS-1–2 | 4 | 10.0 | t. a. | 0.4 | 1.8 | 18.4 | 99.3 |
| 2 | Cu-CN/TS-1–2 | 4 | 4.1 | 0.9 | t. a. | 0.9 | 8.4 | 91.3 |
| 3 | Ni-CN/TS-1–2 | 4 | 1.8 | t. a. | t. a. | t. a. | 20.0 | 16.1 |
| 4 | Zn-CN/TS-1–2 | 4 | 1.2 | t. a. | t. a. | t. a. | 47.6 | 3.6 |
| 5 | Co-CN/TS-1–2 | 4 | 1.0 | t. a. | t. a. | t. a. | 44.4 | 2.8 |

[a] Reaction conditions, see Section 2.

and the integration of Fe-CN onto the TS-1 support greatly increase the formation of •OH-radicals, which are beneficial for the benzene conversion to phenol in the presence of $H_2O_2$ with visible light. This phenomenon is consistent with the experimental results.

## 4. Conclusion

In summary, Fe-CN/TS-1 composite materials were prepared by a facial thermal polymerization approach using dicyandiamide, metal chloride as precursors and TS-1 as a support. Benzene hydroxylation reaction was employed to evaluate the catalytic/photocatalytic activity of the as-synthesized catalysts. The results show that Fe-CN/TS-1 composite catalysts possess much improved catalytic activities under visible light irradiation, about 9 times and 4 times higher than that of sole Fe-CN and TS-1 catalyst, respectively. Under the optimal conditions, up to 10.0% phenol yield (based on benzene) is obtained by Fe-CN/TS-1–2 sample, with 18.4% phenol selectivity (based on $H_2O_2$).

## Acknowledgements

This work is financially supported by the National Basic Research Program of China (973 Program) (Grant No. 2013CB632405), the National Natural Science Foundation of China (Grant Nos. 21033003 and 21173043), the State Key Laboratory of NBC Protection for Civilian (SKLNBC2013-04K), and the Specialized Research Fund for the Doctoral Program of Higher Education (20133514110003).

## References

[1] M. Tani, T. Sakamoto, S. Mita, S. Sakaguchi, Y. Ishii, Angew. Chem. Int. Ed. 44 (2005) 2586–2588.
[2] H.J.H. Fenton, J. Chem. Soc. Trans. 65 (1894) 899–910.
[3] D. Bianchi, R. Bortolo, R. Tassinari, M. Ricci, R. Vignola, Angew. Chem. Int. Ed. 39 (2000) 4321–4323.
[4] S. Ito, A. Mitarai, K. Hikino, M. Hirama, K. Sasaki, J. Org. Chem. 57 (1992) 6937–6941.
[5] K. Otsuka, I. Yamanaka, K. Hosokawa, Nature 345 (1990) 697–698.
[6] B. Lee, H. Naito, T. Hibino, Angew. Chem. Int. Ed. 50 (2011) 1–6.
[7] B. Lee, H. Naito, M. Nagao, T. Hibino, Angew. Chem. Int. Ed. 51 (2012) 1–6.
[8] O. Shoji, T. Kunimatsu, N. Kawakami, Y. Watanabe, Angew. Chem. Int. Ed. 52 (2013) 1–5.
[9] T. Kusakari, T. Sasaki, Y. Iwasawa, Chem. Commun. 8 (2004) 992–993.
[10] S.Q. Song, H.X. Yang, R.C. Rao, H.D. Liu, A.M. Zhang, Appl. Catal., A 375 (2010) 265–271.
[11] Y. Li, Z. Feng, R.A. van Santen, E.J.M. Hensen, C. Li, J. Catal. 255 (2008) 190–196.
[12] L.V. Pirutko, V.S. Chernyavsky, A.K. Uriarte, G.I. Panov, Appl. Catal., A 227 (2002) 143–157.
[13] R. Bal, M. Tada, T. Sasaki, Y. Iwasawa, Angew. Chem. Int. Ed. 45 (2006) 448–452.
[14] Y.Y. Gu, X.H. Zhao, G.R. Zhang, H.M. Ding, Y.K. Shan, Appl. Catal., A 328 (2007) 150–155.
[15] M. Tada, R. Bal, T. Sasaki, Y. Uemura, Y. Inada, S. Tanaka, M. Nomura, Y. Iwasawa, J. Phys. Chem. C 111 (2007) 10095–10104.
[16] K. Ohkubo, T. Kobayashi, S. Fukuzumi, Angew. Chem. Int. Ed. 50 (2011) 8652–8655.
[17] K. Ohkubo, A. Fujimoto, S. Fukuzumi, J. Am. Chem. Soc. 135 (2013) 5368–5371.
[18] S. Niwa, M. Eswaramoorthy, J. Nair, A. Raj, N. Ito, H. Shoji, T. Namba, F. Mizukami, Science 295 (2002) 105–107.
[19] H. Ehrich, H. Berndt, M. Pohl, K. Jähnisch, M. Baerns, Appl. Catal., A 230 (2002) 271–280.
[20] G.I. Panov, A.S. Kharitonov, V.I. Sobolev, Appl. Catal., A 98 (1993) 1–20.
[21] E.J.M. Hensen, Q. Zhu, R.A. van Santen, J. Catal. 220 (2003) 260–264.
[22] A. Ribera, I.W.C.E. Arends, S. de Vries, J. Pérez-Ramírez, R.A. Sheldon, J. Catal. 195 (2000) 287–297.
[23] X.F. Chen, J.S. Zhang, X.Z. Fu, M. Antonietti, X.C. Wang, J. Am. Chem. Soc. 131 (2009) 11658–11659.
[24] K.S. Pillai, J.F. Jia, W.M.H. Sachtler, J. Catal. 264 (2004) 133–139.
[25] B.S. Rana, B. Singh, R. Kumar, D. Verma, M.K. Bhunia, A. Bhaumik, A.K. Sinha, J. Mater. Chem. 20 (2010) 8575–8581.
[26] P.T. Tanev, M. Chibwe, T.J. Pinnavaia, Nature 368 (1994) 321–323.
[27] L. Balducci, D. Bianchi, R. Bortolo, R. D' Aloisio, M. Ricci, R. Tassinari, R. Ungarelli, Angew. Chem. Int. Ed. 42 (2003) 4937–4940.
[28] P. Borah, X. Ma, K.T. Nguyen, Y.L. Zhao, Angew. Chem. Int. Ed. 51 (2012) 1–7.
[29] G.D. Ding, W.T. Wang, T. Jiang, B.X. Han, H.L. Fan, G.Y. Yang, ChemCatChem 5 (2013) 192–200.
[30] D. Barbera, F. Cavani, T. D'Alessandro, G. Fornasari, S. Guidetti, A. Aloise, G. Giordano, M. Piumetti, B. Bonelli, C. Zanzottera, J. Catal. 275 (2010) 158–169.
[31] A. Bhaumik, P. Mukherjee, R. Kumar, J. Catal. 178 (1998) 101–107.
[32] T.D. Bui, A. Kimura, S. Ikeda, M. Matsumura, J. Am. Chem. Soc. 132 (2010) 8453–8458.
[33] T.D. Bui, A. Kimura, S. Higashida, S. Ikeda, M. Matsumura, Appl. Catal., B 107 (2011) 119–127.
[34] Y. Chen, J.S. Zhang, M.W. Zhang, X.C. Wang, Chem. Sci. 4 (2013) 3244–3248.
[35] G. Zhang, J. Yi, J. Shim, J. Lee, W. Choi, Appl. Catal., B 102 (2011) 132–139.
[36] Y. Ide, M. Matsuoka, M. Ogawa, J. Am. Chem. Soc. 132 (2010) 16762–16764.
[37] P.F. Zhang, Y.T. Gong, H.R. Li, Z.R. Chen, Y. Wang, RSC Adv. 3 (2013) 5121–5126.
[38] X.C. Wang, K. Maeda, A. Thomas, K. Takanabe, G. Xin, J.M. Carlsson, K. Domen, M. Antonietti, Nat. Mater. 8 (2008) 76–82.
[39] J.S. Zhang, M.W. Zhang, R.Q. Sun, X.C. Wang, Angew. Chem. Int. Ed. 51 (2012) 10145–11109.
[40] X.C. Wang, K. Maeda, X.F. Chen, K. Takanabe, K. Domen, Y.D. Hou, X.Z. Fu, M. Antonietti, J. Am. Chem. Soc. 131 (2009) 1680–1681.
[41] Y.J. Cui, Z.X. Ding, X.Z. Fu, X.C. Wang, Angew. Chem. Int. Ed. 51 (2012) 1–6.
[42] Z.Z. Lin, X.C. Wang, Angew. Chem. Int. Ed. 52 (2013) 1735–1738.
[43] F.Z. Su, S.C. Mathew, G. Lipner, X.Z. Fu, M. Antonietti, S. Blechert, X.C. Wang, J. Am. Chem. Soc. 132 (2010) 16299–16301.
[44] X.-H. Li, J.-S. Chen, X.C. Wang, J.H. Sun, M. Antonietti, J. Am. Chem. Soc. 133 (2011) 8074–8077.
[45] J.L. Lin, Z.M. Pan, X.C. Wang, ACS Sustainable Chem. Eng. (2014), doi.org/10.1021/sc4004295.
[46] Y.J. Cui, Z.X. Ding, P. Liu, M. Antonietti, X.Z. Fu, X.C. Wang, Phys. Chem. Chem. Phys. 14 (2012) 1455–1462.
[47] Z.X. Ding, X.F. Chen, M. Antonietti, X.C. Wang, ChemSusChem 4 (2011) 274–281.
[48] X.C. Wang, X.F. Chen, A. Thomas, X.Z. Fu, M. Antonietti, Adv. Mater. 21 (2009) 1609–1612.
[49] M. Choi, H.S. Cho, R. Srivastava, C. Venkatesan, D. Choi, R. Ryoo, Nat. Mater. 5 (2006) 718–723.
[50] E. Gianotti, C. Bisio, L. Marchese, M. Guidotti, N. Ravasio, R. Psaro, S. Coluccia, J. Phys. Chem. C 111 (2007) 5083–5089.
[51] J.S. Zhang, X.F. Chen, K. Takanabe, K. Maeda, K. Domen, J.D. Epping, X.Z. Fu, M. Antonietti, X.C. Wang, Angew. Chem. Int. Ed. 49 (2010) 441–444.
[52] G.G. Zhang, X.C. Wang, J. Catal. 307 (2013) 246–253.
[53] G. Liu, C.H. Sun, L.N. Cheng, Y.G. Jin, H.F. Lu, L.Z. Wang, S.C. Smith, G.Q. Lu, H.-M. Cheng, J. Phys. Chem. C 113 (2009) 12317–12324.
[54] W.J. Li, D.Z. Li, W.J. Zhang, Y. Hu, Y.H. He, X.Z. Fu, J. Phys. Chem. C 114 (2010) 2154–2159.